Engineering Transactions, **67**(3): 311–331, 2019, doi: 10.24423/EngTrans.1005.20190815
Polish Academy of Sciences • Institute of Fundamental Technological Research (IPPT PAN)
Université de Lorraine • Poznan University of Technology

Comparison Between Numerical Analysis and Actual Results for a Pull-Out Test

Jakub GONTARZ[1)*], Jerzy PODGÓRSKI[1)], Józef JONAK[2)]
Marek KALITA[3)], Michał SIEGMUND[3)]

[1)] *Faculty of Civil Engineering and Architecture*
Lublin University of Technology
Lublin, Poland
[*]Corresponding Author e-mail: j.gontarz@pollub.pl

[2)] *Faculty of Mechanical Engineering*
Lublin University of Technology
Lublin, Poland

[3)] *KOMAG Institute of Mining Technology*
Gliwice, Poland

The paper describes a computer analysis of the pull-out test used to determine the force needed to pull out a fragment of rock and the shape of this broken fragment. The analyzed material is sandstone and porphyry. The analysis included a comparison of different methods of propagation of cracks in the Abaqus computer program using the Finite Element Method. The work also contains a description of laboratory tests and analytical considerations.

Key words: pull-out test; rock mechanics; fracture mechanics; numerical modeling of fracture.

1. Introduction

The authors of this paper have attempted to analyze and numerically simulate the rock fracturing test using a pre-installed self-cutting anchor – so-called pull-out test. The described test aims to extract the largest possible fragment of rock together with the anchor. This is a different application of the anchor from its standard purpose because it is designed so as not to destroy the material in which it is mounted when it is attempted to pull it out by force equal to its bearing capacity. The research consisted of finding the parameters of the selected material – sandstone from the Braciszów quarry. Next, a pull-out test was modeled in the Simulia Abaqus FEA system and computer analysis was performed

using X-FEM elements, which are elements simulating the crack independent of the finite element mesh. The results obtained in the calculations were compared with the pull-out tests performed on real rock. The aim of the described research is to find a way to calculate the force of pulling out the anchor for any material and for any depth of anchoring. The reason why this topic was raised is the problem of mining rescue. In some cases in mines, the destruction of rocks with explosives is impossible, which is why the idea of destroying rocks by pulling the anchor was born.

HILTI HDA-P M20 × 250/100 anchor (Fig. 1) used for this test is normally mounted at a depth of 25 cm [1], but for *in-situ* tests it was mounted at a depth of 6 cm to 12 cm due to the avoidance of cases where the anchor was destroyed without breaking the rock.

FIG. 1. Pre-set undercut Hilti HDA-P anchor.

To mount this anchor it is placed in a hole prepared in the anchored surface. Then, a drill is attached to the anchor, and while drilling, the anchor undercuts the rock with deflecting elements. Scheme of the anchor mounting is shown in Fig. 2. Fixing the anchor, therefore, consists of the contact between the material and the undercut, not the anchor side. So the contact area is relatively small.

a) b)

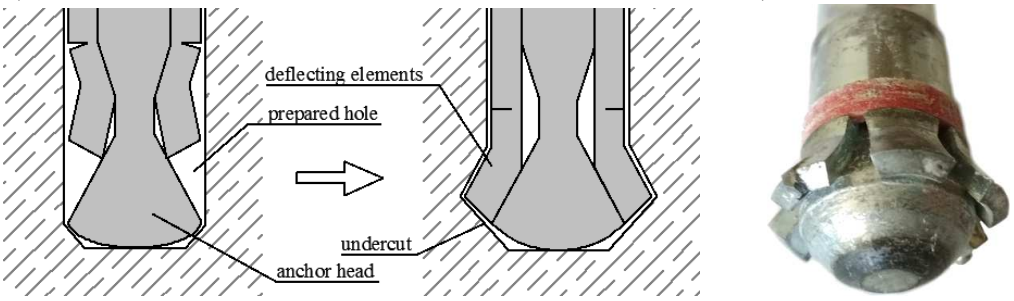

FIG. 2. a) Scheme of mounting the anchor, b) head of the used anchor.

The authors made an attempt to estimate the critical force and determine the size of a pulled-out rock fragment with X-FEM computer method of crack modeling in program Abaqus. The analyses focused on sandstone obtained from a quarry in Braciszów in Poland but there are also some samples of porphyry from a quarry in Zalas in Poland. The main purpose of this work is to compare the results obtained for different methods of the application the load in FEA

system and the future goal is to find the universal method of finding the pulling-out force for various test parameters.

A similar issue is described in paper Contrafatto and Cosenza [2], but instead of undercut anchors, steel bars fixed inside surface layers of the examined material are used. Thus the characteristic of the pull-out test is completely different from those described in the above paper.

In other works [3] the capacity of adhesive anchors was examined. Also in paper [4], fixed anchors surrounded by plastic pipe were investigated. The characteristics of these tests are similar to those described in the presented work, but here the same anchor was used several times and the construction of the anchor is different.

2. Description of the task

2.1. FEA model

Simulia Abaqus FEA system was used for calculations. Here the X-FEM method was used for modeling the crack propagation. The pull-out test was modeled in 2D space as an axially symmetrical task. The computational model is presented in Fig. 3, where h_0 is the depth of the anchorage. The boundary conditions were modeled on the right and bottom edge. The size of the model was assumed to be large enough so that the boundary conditions did not affect the result. Element mesh size varied from 2 mm to 10 mm, dense mesh of elements was located in the area of the expected crack propagation.

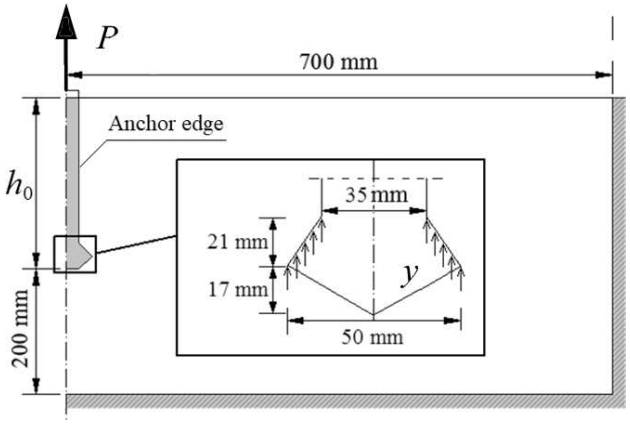

Fig. 3. Scheme of the task.

The sandstone material was modeled as linear-elastic with Young's modulus $E = 15.744$ GPa, Poisson's ratio $\nu = 0.251$, tensile strength $f_t = 7.74$ MPa,

and the critical strain energy release rate $G_{Ic} = 0.306$ N/mm. The laboratory tests from which these parameters were obtained are described in the further subsection. Tensile strength f_t is also the stress that initiates the crack.

The load was simulated by several different methods. The first method is that there is no anchor in the model, but the load was simulated by the vertical displacement applied at the anchor undercut (see Fig. 3). This method was divided into two variants. First – with horizontal blocking on the anchor edge, second – without this blocking. Next method is with an anchor in the model. The load was simulated by vertical displacement applied on the upper edge of the anchor, and there exists the contact between the anchor and sandstone, with 5 different friction coefficients: $\mu = 0.01$, 0.1, 0.2, 0.5, and 1.0. There is no possibility to determine the exact friction coefficient between these two materials because in this test the rock under heavy load is crushed, but still, this crushed part transfers the load further.

2.2. Estimation of critical force

In the initial phase of the analyzes, the authors attempted to analytically estimate the maximum force of breaking the rock fragment. For this purpose, the task has been simplified to that shown in Fig. 4.

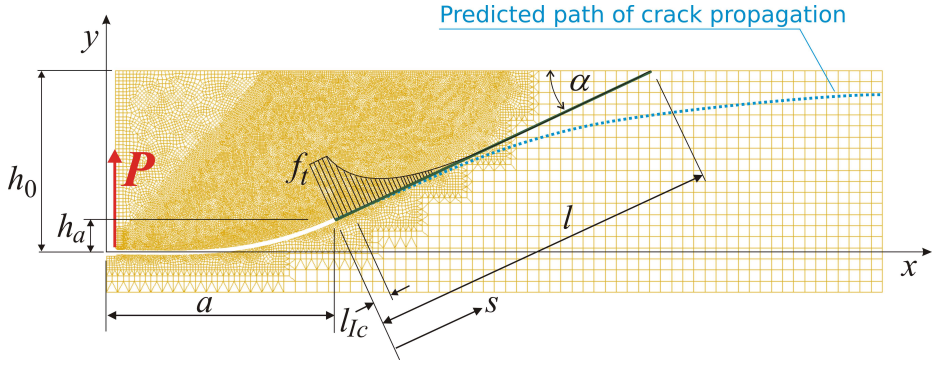

FIG. 4. Scheme for estimating the critical force P.

The critical force is determined by the sum of vertical reactions in nodes with applied displacement, both in the case of load specified in the place of contact of two materials and for the load at the end of the anchor.

For simplicity, it was assumed that the shape of the detached fragment of the rock is approximately conical, which isn't consistent with the following computer simulations, but these considerations only refer to finding the critical force, so only the angle α around which the greatest strength has been achieved in the computer tests is significant. The angle of the crack is $\alpha = 21°$, and it was

adopted as a mean from computer tests and tests on actual rock described in the following subsections, obtained when the maximum strength is achieved.

The distribution of tensile stresses from the crack tip to the hypothetical point of fracture of the rock fragment was adopted on the basis of the Barenblatt hypothesis – "cohesive zone" [5]. This hypothesis, thanks to the introduction of the "cohesive zone" in the crack tip area, allows taking into account the microcracks development that precedes propagation of a discrete crack. At the cohesive zone length, l_{Ic} (2.1), it has the shape of a rectangle with the intensity of equal tensile strength, outside the zone the stresses decrease, reaching the zero value near the rock surface. For simplicity, it was assumed that the normal stress distribution curve in this segment is described by the function of the type $[1 - \tanh(Ax^d)]$ (Fig. 5), which roughly corresponds to the values obtained from the numerical model. For different steps of the calculation (different crack length a) it turned out that the stress field is similar for these steps. The cohesive zone length l_{Ic} is calculated from the equation:

$$l_{Ic} = M \cdot E \cdot \frac{G_{Ic}}{\sigma_{Ic}^2}, \tag{2.1}$$

where M is the parameter for the chosen cohesive zone model, σ_{Ic} is the stress in the cohesive zone. For brittle materials, there is Barenblatt model with $M = \pi/8$ [5], and in this case $\sigma_{Ic} = f_t$. For the above parameters $l_{Ic} = 25.6$ mm.

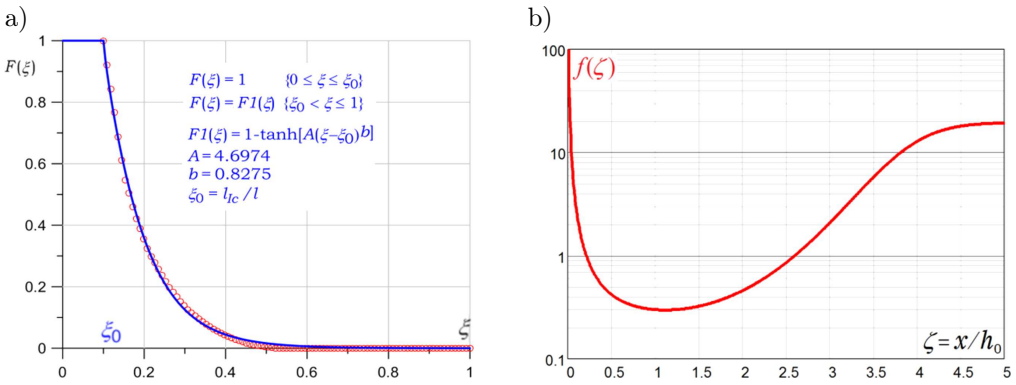

FIG. 5. Approximation functions: a) stress field near the crack tip approximated by the $\tanh(\xi)$ function (solid line) and point of normalized stress values calculated with the FEA model, b) stress intensity factor function $f(\zeta)$ calculated for predicted crack path $y(\zeta)$.

The value of P force is calculated from the equilibrium condition of vertical forces:

$$P = \int_S \sigma_n \cos\alpha \, \mathrm{d}S, \tag{2.2}$$

where σ_n is the stress normal to the surface of the cone and S is the area of the cone's side surface. The tangent components of stress have been omitted here due to their very small values.

After some transformations, Eq. (2.2) takes the form:

$$P = 2\pi\, l \cos\alpha \int_0^l \sigma_n x \,\mathrm{d}s = 2\pi\, l^2 \cos\alpha \int_0^1 \sigma_n \frac{x}{l}\,\mathrm{d}\xi, \tag{2.3}$$

where $\xi = s/l$. After substitution $x = a + s\cos\alpha$ and $\sigma_n = f_t F(\xi)$ we get:

$$P = 2\pi\, l^2 f_t \cos\alpha \int_0^1 F(\xi)\left(\frac{a}{l} + \xi\cos\alpha\right)\mathrm{d}\xi. \tag{2.4}$$

The graph of the $F(\xi)$ function is shown in Fig. 5.

The predicted maximum value of force occurs in the place where the range of the crack is approximately equal to the depth of the anchorage ($a \approx h_0 =$ 100 mm, $h_a = 20$ mm) and $P_{\max} = 290.84$ kN. This estimation gives the upper bound of critical force and unfortunately has a disadvantage resulting from the strong dependence of $P_{\max}$ on the a and h_a parameters. The values a and h_a used in this estimation, result from many numerical tests in which the maximum value of P, required for the crack propagation, was obtained.

A much better estimation was obtained on the basis of considerations arising from the condition that must be fulfilled by the force required to crack propagation:

$$K_I = \frac{P}{\sqrt{h^3}} f(\zeta), \tag{2.5}$$

where K_I is the stress intensity factor in the first mode of cracking, $f(\zeta)$ is a dimensionless function depending on the shape of the crack path, and $\zeta = x/h_0$. This function was determined using the finite element method assuming that the shape of the crack path is described by the equation:

$$y(\zeta) = h_0\left[1 - \frac{1}{1+B}\left(\frac{1}{e^{(d\cdot\zeta)^c}} + B\right)\right] \tag{2.6}$$

which with constants $B = 0.05$, $c = 3$, $d = 0.4$ corresponds to the results of the *in situ* tests (see dotted line in Fig. 4). The graph of the function $f(\xi)$ is shown in Fig. 5b. The minimum value of this function is obtained for $\zeta = 1.12$ and is $f_{\min} = 0.2962$. The critical value of the stress intensity factor K_{Ic} is calculated

on the basis of experimentally obtained G_{Ic} – critical values of the strain energy release rate (comp. Eq. (3.3)): $K_{Ic} = \sqrt{E\,G_{Ic}}$ and hence:

$$P_{\max} = \frac{K_{Ic}\sqrt{h_0^3}}{f_{\min}}, \tag{2.7}$$

which, for the parameters described above, gives the value $P_{\max} = 233.5$ kN.

This value is also the upper bound of $P_{\max}$, which results from the arbitrarily adopted form of the crack path but also from the neglecting the shear stress effect, and therefore the K_{II} value of the stress intensity factor. This value is already, as shown later in this paper, very close to the results of computer simulations and *in situ* tests.

3. Material parameters

Creating a correct numerical model of the "pull-out" test requires precise material data. A series of laboratory tests were carried out in this point, the aim of which was to determine Young's modulus, Poisson's ratio, compressive and tensile strength as well as the strain energy release rate.

3.1. Compression test

Fourteen cubic samples of dimension $7 \times 7 \times 7$ cm were used to determine material parameters. They were used to calculate Young's modulus and Poisson's ratio during compression tests with the use of extensometers measuring lateral deformations. Then the compressive strength was obtained from the destructive compression test performed on the same samples.

Photograph of these tests is shown in Fig. 6. On the left side, there is visible a displacement sensor which measures the vertical deformations, and on the right side, there is an extensometer that measures the horizontal deformations. It is mounted on steel plates glued to the opposite sides of samples.

Fig. 6. Compression test with an extensometer.

The Young modulus was calculated from the equation below:

$$E = \frac{h \cdot \kappa}{A}, \tag{3.1}$$

where h is the height of the sample, A is the area of the horizontal cross-section of the sample and κ is the slope of the curve of a compressive force to vertical deformations dependence (Fig. 7a). There were 14 cubic samples named K1–K14, but some tests were unsuccessful. The Young's modulus varied from 10.1359 to 24.7678 GPa. The mean value was 15.7449 GPa with a standard deviation of 4.8192 GPa (31% of the mean value).

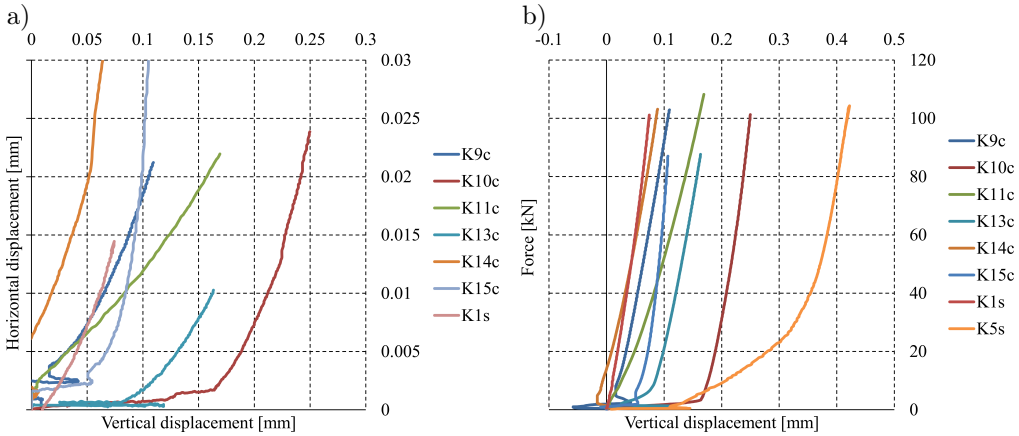

FIG. 7. Results from the compression tests: a) relation between the force and vertical displacement, b) relation between horizontal and vertical displacement of the sample.

The Poisson's ratio was estimated as the ratio of horizontal deformations obtained from the extensometer to vertical deformations obtained from the displacement sensor (Fig. 7b). The calculated Poisson's ratio varied from 0.1199 to 0.2909. The mean value was 0.2025 with a standard deviation of 0.0694 (34% of the mean value). The compressive strength was obtained from the standard method as the ratio of the destructive force to the area of the horizontal cross-section of the sample. The mean value was 187.23 MPa with a standard deviation of 18.46 MPa (∼10% of the mean value).

3.2. Beam bending test

Critical stress intensity factor is a material characteristic. It specifies the amount of stress concentration at the crack tip. There are three main modes of cracks. In the case of the problem described in this paper, the most appropriate mode is mode I, which occurs when opening a crack caused by the tensile force perpendicular to the crack.

The authors have performed a three-point bending test on notched beams to calculate the stress intensity factor in mode I and then the critical strain energy release rate in mode I.

The three-point bending tests of sandstone beam samples were made. This test was performed on specimens with the notch in the middle of the span. Figure 8 shows how this test works, and Fig. 9 shows the photo taken during the laboratory test.

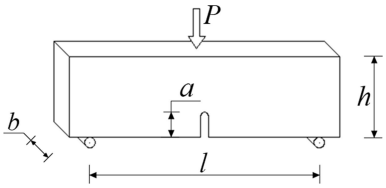

FIG. 8. Scheme of the three-point bending test with notches.

FIG. 9. Three-point bending test for notched beams.

There are several methods for calculating the stress intensity factor in fracture mode I with three-point bending test [6, 7]. In this work the ASTM formula proposed by BROWN and SRAWLEY [8] was used:

$$K_{Ic} = \frac{3P_c l\sqrt{\pi a}}{2h^2 b}\left[1.090 - 1.735\frac{a}{h} + 8.20\left(\frac{a}{h}\right)^2 - 14.18\left(\frac{a}{h}\right)^3 + 14.57\left(\frac{a}{h}\right)^4\right]. \tag{3.2}$$

P_c value used in this equation is the force that initiates the crack in this bending test, a is the length of the notch, h – the height of the beam, b – the width of the beam, l – the length of the beam.

Six samples were subjected to these tests, for which the critical value of the stress intensity factor K_{Ic} was calculated. The average value of K_{Ic} was 69.184 N/mm$^{3/2}$, which is close to the factors obtained for similar materials. The standard deviation was 5.504 N/mm$^{3/2}$ (8% of the mean value).

The critical strain energy release rate in mode I was calculated from the equation:

$$G_{Ic} = \frac{K_{Ic}^2}{E}. \tag{3.3}$$

Its value is 306 N/m, with standard deviation 48 N/m (i.e. 16% of the mean value). Similar values were obtained for different rocks by HASANPOUR and CHOUPANI [10].

3.3. Quasi-Brazilian test

The authors also made a quasi-Brazilian test on cubes. Typically tests of traction during splitting are performed on cylindrical samples, but they are hard to obtain from such material as an analyzed here, so the FEA Abaqus system was used to find the stress field and then the tensile strength for cubic samples. Tensile strength was calculated using the formulas given in the authors' earlier study [11]. The Ottosen-Podgórski criterion was used for generalized plane strain state. Tensile strength was calculated from the following equation:

$$f_t = \frac{\sigma_{\max}}{\rho}, \tag{3.4}$$

where $\sigma_{\max}$ is the tensile stress in the center of the sample, obtained from own numerical analyzes, ρ is the coefficient depending on the ratio of tensile and compressive stress and the chosen failure criterion for material in a complex stress state [11]. For the tested rocks, the value of this coefficient was $\rho \approx 0.96$. Stress field in the generalized plane strain state was determined by the finite element method. This issue was also analyzed by J.N. GOODIER [12], who determined stress distributions using an analytical method. Values given by Goodier concern rectangular blocks with proportions height to width equal 2, 1, and 0.5.

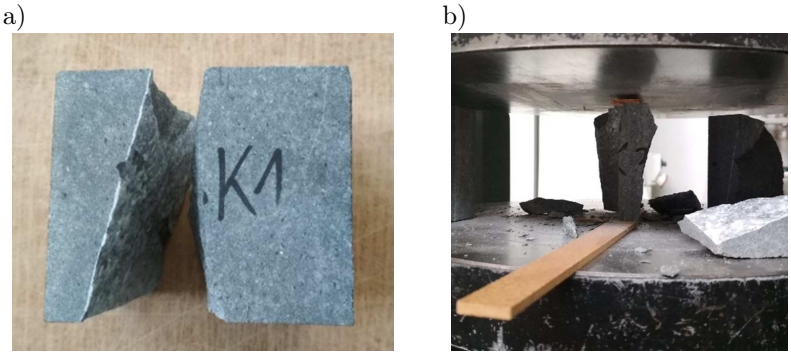

FIG. 10. The quasi-Brazilian test.

For 4 examined samples the tensile strength was 12.89 MPa with a standard deviation of 3.72 MPa (29% of the mean value).

Figure 10 presents the samples after exemplary tests. Here the heterogeneity of the examined material can be seen.

4. Computer simulations

4.1. Comparison of different simulation approaches

The above material parameters were used to model the test in Abaqus for a 9 cm anchoring. The authors have used the X-FEM method of crack propagation. Extended Finite Element Method is a method of simulating a fracture in the Finite Element Method, which is independent of the mesh. Modification of the shape function of an element allows the finite element to be separated anywhere [13], so the element mesh does not have to be too dense.

Another commonly used method of simulating the fracture in a brittle material is the continuous-discontinuous method, which involves introducing weakening material in the area of crack propagation [14]. This method is particularly popular in the modeling of concrete fracture [15]. This "smeared crack" method is used in the procedures implemented in the commercial FEA codes ANSYS and Simulia Abaqus.

Authors decided to use in this work the discrete crack simulation method, which is also implemented in the Abaqus code, using the Barenblatt's "cohesive zone" model. In this model crack initiation refers to the beginning of the degradation of a cohesive response in an enriched X-FEM element. The degradation process begins when stresses or strains meet certain crack initiation criteria. Crack initiation criteria are available based on the following built-in Abaqus/Standard models: the maximum principal stress criterion, the maximum principal strain criterion, the maximum nominal stress criterion, the maximum nominal strain criterion, the quadratic traction-interaction criterion, and the quadratic separation-interaction criterion. An additional crack is introduced or crack length of an existing gap is carried on after an equilibrium increment when the crack propagation criterion $f = 1.0$ [16]. In the above example, the simplest criterion for crack initiation is chosen, which is the maximum principal stress damage – when the tensile stress exceeds the tensile strength value. The evolution of damage can be determined on the basis of fracture energy or displacement at failure. In this simulation, energy is the most suitable choice because the critical rate of strain energy release has been determined from laboratory tests. The linear softening curve was chosen in damage evolution of the material [9].

As described previously, 7 methods of applying the pull-out force were checked:

- without anchor, locked horizontal displacement,
- without anchor, with horizontal displacement,
- with an anchor, friction coefficient $\mu = 0.01$,
- with an anchor, friction coefficient $\mu = 0.1$,
- with an anchor, friction coefficient $\mu = 0.2$,
- with an anchor, friction coefficient $\mu = 0.5$,
- with an anchor, friction coefficient $\mu = 1.0$.

Figures 11 and 12 show examples of finite element mesh and a map of principal stresses calculated using a model created in the Simulia Abaqus FEA system. Figure 11 shows one of the models before applying the load. The view of the model with crack simulation is shown in Fig. 12.

As can be seen, the crack starts to propagate as expected, but the crack near the top edge begins to distort and return. For various program settings and different meshes, it was not possible to cause the crack to go through to the end. Probably there is a stress state with which the Abaqus program can't cope and can't decide where to lead the crack. This is related to the limitations of X-FEM in Abaqus. The pull-out force at the beginning grows and then decrease after reaching the radius of the extracted fragment, approximately equal to the depth of the anchor (h_0). Figure 13 is the graph showing how the force was changing during the crack growth in simulations. As can be seen, there is a very big difference between the results. The maximum force varies from about 100 kN to 220 kN.

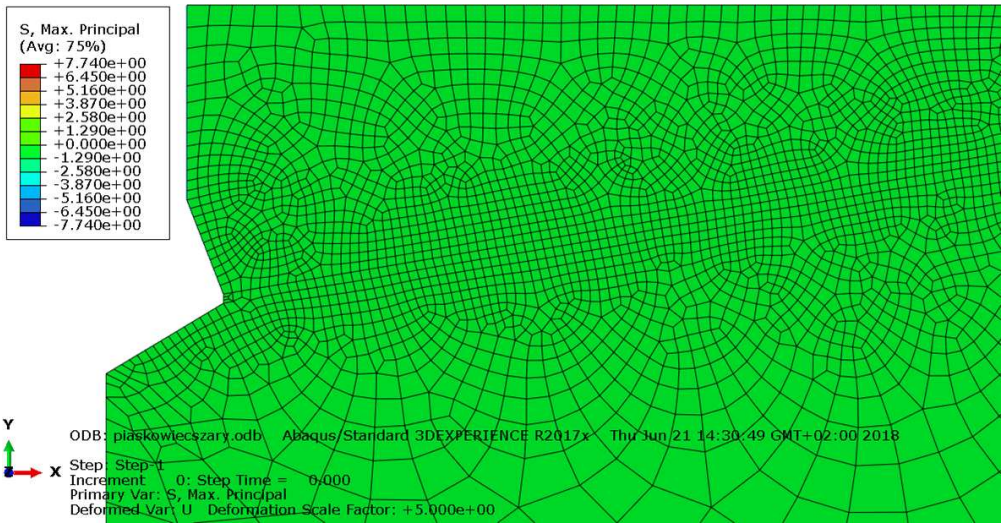

FIG. 11. Model of the test before applying the load.

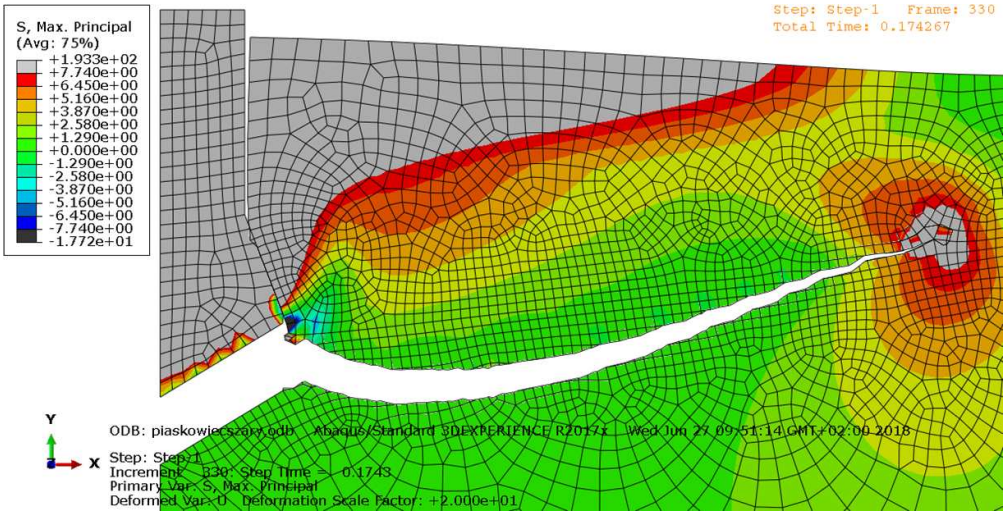

FIG. 12. Last step of calculation from the simulation with an anchor and friction coefficient $\mu = 0.2$.

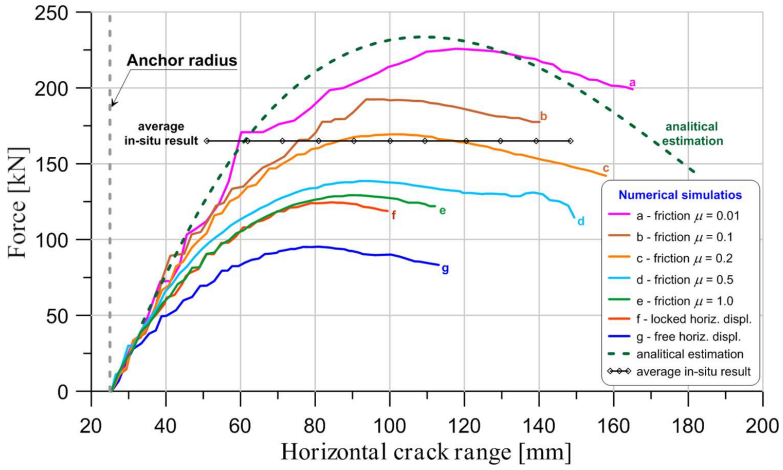

FIG. 13. Graph of the critical force dependence on the friction coefficient. Result of the analytical critical force estimation is marked with a dashed line, the horizontal black line shows the average value of the critical force from in-situ tests.

In Fig. 14 crack paths for different methods are shown. Here the results for simulations without anchor are so unnatural, that they can't be taken into account further. Nevertheless, the results for simulations with the anchor are also very different to each other. Also, the maximum force is obtained in different places, with different crack length. This means that the model and friction coefficient should be chosen very carefully, it is quite difficult due to the fact that

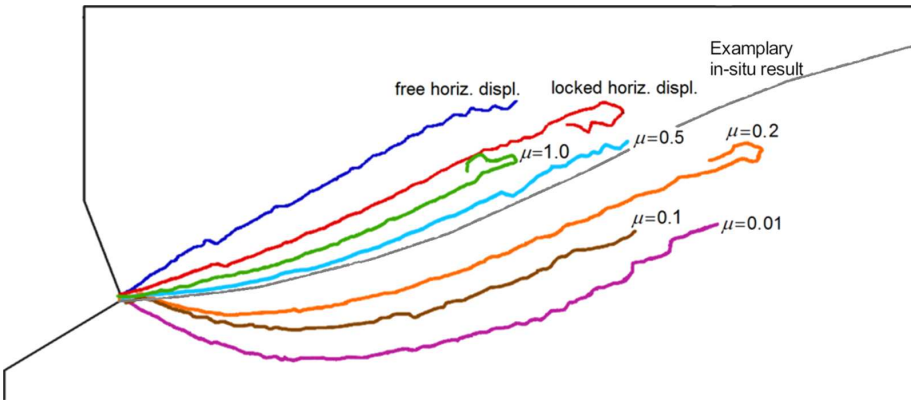

FIG. 14. Crack paths for different methods of load applying.
Colour scheme is the same as in Fig. 13.

the material crushes in contact with the anchor. As it will be proved in the next chapter, the shape closest to reality is the one for the friction coefficient $\mu = 0.2$.

It can be seen that the path of the crack at the very end behaves irregularly in all models. It should also be noted that the line for the in-situ test is approximate because it is physically impossible to acquire such information during the test. This test is described in the next section.

The main conclusion from the above analyses is that anchors should not be omitted in the analyzes, however, different friction coefficients have a very big influence on the result, both on the maximum force and the crack path.

4.2. Comparison of different mesh sizes

The authors decided to examine the dependence of the results on the mesh size. For this purpose, four variants were modeled, all with friction coefficient $\mu = 0.1$, but with different densities of the mesh along the expected crack line: 2 mm, 3 mm, 5 mm and 10 mm. For 10 mm mesh size, the maximum force $P_{\max} = 195$ kN was obtained, for 5 mm mesh $P_{\max} = 201$ kN, for 3 mm $P_{\max} = 192$ kN, and for 2 mm $P_{\max} = 205$ kN. It can be concluded that the 5 and 10 mm dimensions of the element's side are too large because they cause too large disturbances in the stress distribution around the crack tip. On the other hand, the calculations for the 2 mm mesh were discontinued because the simulation progress stopped for a long time. The conclusion is that choosing the right grid size is important, but the difference between the results for the highest and lowest mesh density is small and amounts to about 6%. In addition, the lines of the crack in the correct part of the simulation are very similar to each other, which can be seen in Fig. 15. The fact that the size of the FE mesh has negligible significance in the X-FEM method agrees with the literature [17].

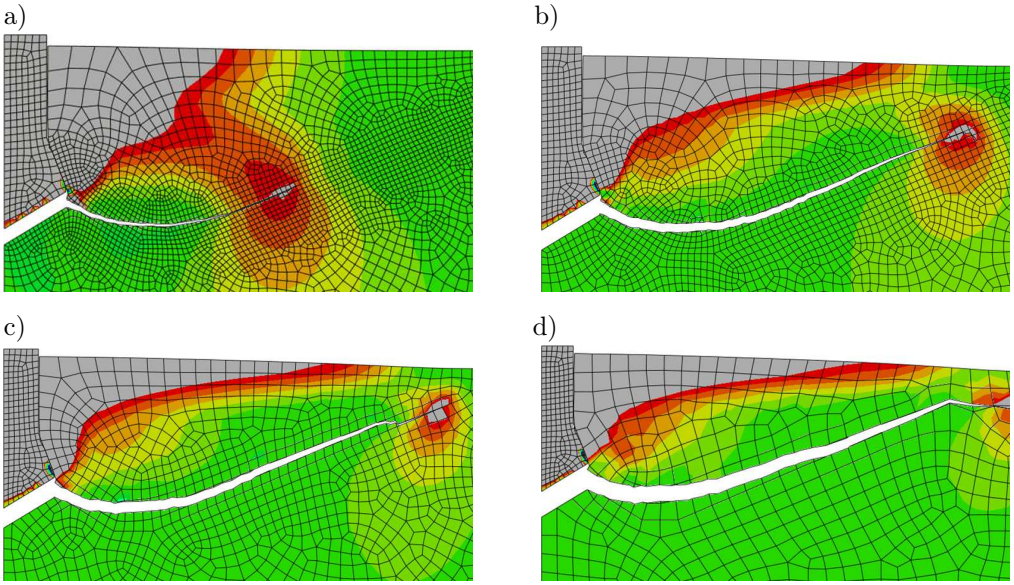

FIG. 15. Comparison of the crack path shape for various mesh densities: a) the smallest mesh size = 2 mm, b) 3 mm, c) 5 mm, d) 10 mm.

4.3. Impact of tensile strength and fracture energy on the result'

An important issue is to check the impact of tensile strength and critical fracture energy on the crack path and maximum value of the acting force. It was decided to examine 11 additional options: with f_t = (0.60, 0.65, 0.70, ..., 0.90, 1.15, 1.25, 1.40, 1.50)f_{t0} of standard tensile strength value, and with 7 additional fracture energy values: G_I = (0.60, 0.75, 0.90, 1.15, 1.25, 1.40, 1.50) G_{I0}. The results of calculations with changed material parameters are shown in Fig. 16.

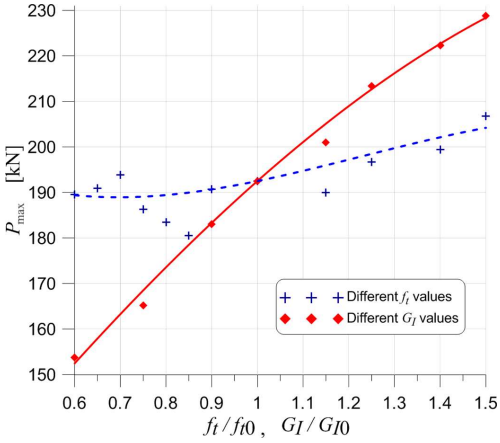

FIG. 16. Dependence of the critical force on tensile strength and fracture energy.

For all new tests crack paths are almost the same with small differences. In some of the simulations, the crack went further, in others it stopped earlier. But the initial shapes of the crack are so close to each other, that the effect of tensile strength and cracking energy on the size of the pulled-out shape can be neglected. But these parameters have an influence on the maximum force value, which is shown in Fig. 16. As can be seen, the higher the tensile strength or cracking energy, the higher the value of the maximum critical force. This relationship for the fracture energy is almost linear, but for tensile strength the shape of this relationship for unclear reasons is quite unusual. Especially for the reduced values of f_t, implemented in Abaqus algorithm shows visible instability, which is indicated by jumps of the critical force values shown in Fig. 16 at $f_t/f_{t0} < 1$.

4.4. Comparison of the results for different anchoring depths

In the same way as above, the maximum force calculation for different anchoring depths was made. One type of simulation was selected – with an anchor and friction coefficient $\mu = 0.1$. Simulations for anchoring depths $h = 6$ cm, 8 cm, 10 cm, and 12 cm were made. The obtained dependence between the maximum force and the anchoring depth is shown in Fig. 17. "Brenna quarry data" are results from a quarry in Brenna in Poland.

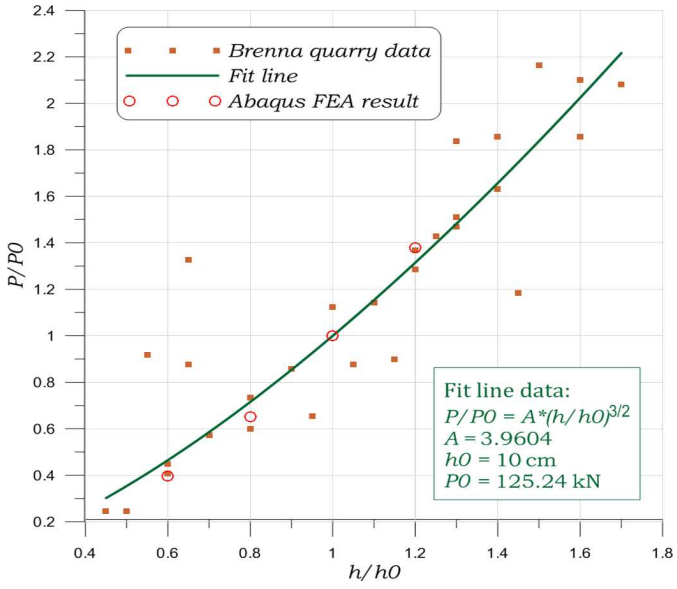

FIG. 17. Dependence between the critical force and the anchoring depth.

This dependence is consistent with the function proposed in the Eq. (2.6) describing the dependence of the stress intensity factor on the anchorage depth

$P_{\max} \sim h_0^{3/2}$, which means that in future considerations it will be easier to estimate the value of pull-out force for different anchor depths. This equation can also be used to estimate the critical value of the stress intensity factor during tests in a quarry or mine:

$$K_{Ic} \cong \frac{P_{\max} f_{\min}}{\sqrt{h_0^3}}, \tag{4.1}$$

where $f_{\min}$ – minimum value of the $f(\zeta)$ function can be set approximately to $\sim$0.3, and h_0 is the depth of the anchorage.

5. In situ pull-out test

Tests in the quarry were also made on the same stone and for the same depth of the anchor (Fig. 19). For three successful tests (P4–P6) performed on sandstone, the average pulling-out force is 162 kN. The relationship between the force and time during the tests is shown in Fig. 18. Inspection of the damaged rock shown in Fig. 20 allowed to state that the shape of the broken fragment is similar to these in the computer simulation, especially for the simulation with the anchor and with friction coefficient $\mu = 0.2$. Visual inspection and measurements of pulled-out fragments allow stating that the range of the crack (cone radius) is about 4 times greater than the anchorage depth. It can also be seen that the rock breaks off at the end of the crack (the crack runs vertically to the surface of the rock).

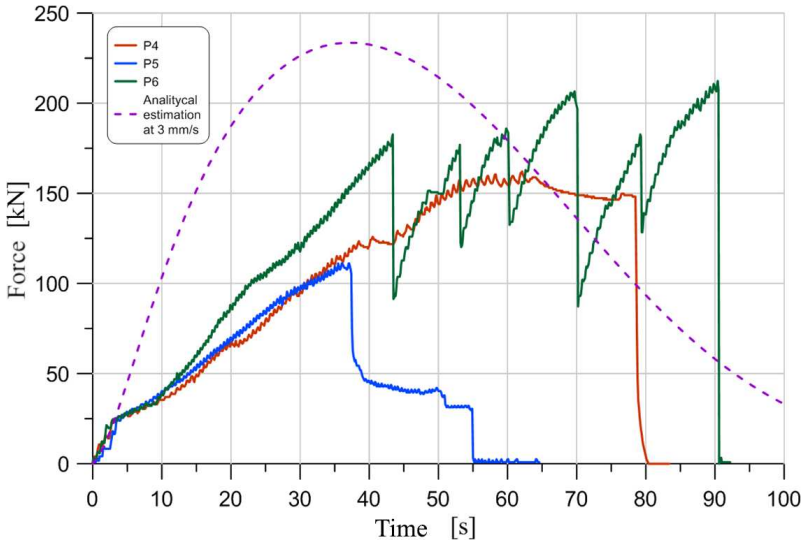

Fig. 18. The relation between the force and time during in-situ tests.

FIG. 19. Pull-out test performed on actual rock.

a)

b)

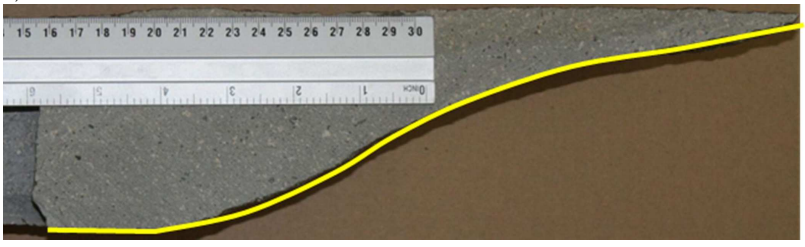

FIG. 20. A cross-section of the actual pull-out sample: a) sandstone, b) porphyry.

Examining one of the pulled-out cones in Fig. 21 it is also possible to explain incorrect crack behavior in computer simulations. It is evident that the width of the pulled-out fragment is different on the circumference. In most places, the rock breaks perpendicular to the surface at the very end. Probably in simulations,

FIG. 21. The shape of the actual pull-out sandstone sample.

there should also be observed such a crack, but the Abaqus program has difficulty in simulating the forking of the crack.

6. SUMMARY

All the maximum force values for different methods that have been achieved are presented below:

- analytical estimation: 233.5 kN,
- Abaqus – locked horizontal displacement: 124.5 kN,
- Abaqus – with horizontal displacement: 95.3 kN,
- Abaqus – friction coefficient $\mu = 0.01$: 225.9 kN,
- Abaqus – friction coefficient $\mu = 0.1$: 190.7 kN,
- Abaqus – friction coefficient $\mu = 0.2$: 169.4 kN,
- Abaqus – friction coefficient $\mu = 1$: 129.2 kN,
- Mean from the in-situ test: 162.0 kN.

All results are very different from each other. Therefore, in the future, it is planned to perform and analyze more laboratory tests on the sandstone from the Brenna quarry, where a few times more pull-out tests have already been carried out. As it was stated before, the results without the anchor are incorrect in relation to models with an anchor as well. The best-obtained result is for simulation with anchor and for friction coefficient between the anchor and the rock $\mu = 0.2$. This is both in terms of the maximum obtained force and the shape of the crack. As can be seen in Figs 13 and 14 the results are very close to the ones for in situ tests. The starting angle of the crack is also nearly the same as for actual results. However, it is not known if this coefficient is correct, especially since in fact it should be variable due to the changes in the rock during the test. Because of the compression, the rock crashes near the area of the contact.

Computer simulations can't be performed to the total breakage of the rock fragment, because before the end the crack begins to behave inconsistently to the test in reality. Fortunately, the maximum force was obtained before the occurrence of this phenomenon, which means that even if this phenomenon continues to occur, it is possible to determine the maximum force. Because of the fact that the Abaqus system has difficulties with the correct determination of the direction of crack propagation, which is particularly visible near the upper bound of the model, the authors plan to implement a special subroutine "Abaqus User Subroutine" in which the own crack propagation criterion will be used. The algorithm implemented in the Abaqus system determines the direction of crack propagation as the maximum principal stress direction in each element in which the crack occurs. The method the authors intend to use is to determine the direction of the crack by finding the gradient direction of the function determining the material effort near the crack tip, as described in [18], as well as other criteria used to predict the direction of crack propagation. The application of these criteria will allow indicating the appropriate method of the simulation the pull-out task in field conditions.

Acknowledgments

This research (for author JG) was sponsored by the Lublin University of Technology Statutory Funds S16/2017 and (for authors JP, JJ, MK, MS) by the Polish National Science Center, project RODEST nr 2015/19/B/ST10/02817.

References

1. European Technical Assessment ETA-99/0009 of 06/01/2015 for Hilti HDA and HDA-R anchor.

2. Contrafatto L., Cosenza R., *Behaviour of post-installed adhesive anchors in natural stone*, Construction and Building Materials, **68**: 355–369, 2014, doi: 10.1016/j.conbuildmat.2014.05.099.

3. Upadhyaya P., Kumar S., *Pull-out capacity of adhesive anchors: An analytical solution*, International Journal of Adhesion and Adhesives, **60**: 54–62, 2015, doi: 10.1016/j.ijadhadh.2015.03.006.

4. Tistel J., Grimstad G., Eiksund G., *Testing and modeling of cyclically loaded rock anchors*, Journal of Rock Mechanics and Geotechnical Engineering, **9**(6): 1010–1030, 2017, doi: 10.1016/j.jrmge.2017.07.005.

5. Barenblatt G.I., *The mathematical theory of equilibrium of crack in brittle fracture*, Advances in Applied Mechanics, **7**: 55–129, 1962, doi: 10.1016/S0065-2156(08)70121-2.

6. Bower A.F., *Applied mechanics of solids*, CRC Press, 2010.

7. Elices M., Guinea G.V.G., Gómez J., Planas J., Gomez J., *The cohesive zone model: advantages, limitations and challenges*, Engineering Fracture Mechanics, **69**(2): 137–163, 2002.

8. Brown W.F., Srawley J.E., *Plane Strain Crack Toughness Testing of High Strength Metallic Materials*, Philadelphia: ASTM International, 1966.

9. van Mier J.G.M., *Fracture processes of concrete*, CRC Press, 1996.

10. Hasanpour R., Choupani N., *Mixed-mode study of rock fracture mechanics by using the modified arcan specimen test*, International Journal of Geotechnical and Geological Engineering, **2**(5): 716–721, 2008.

11. Gontarz J., Podgórski J., *Explanation of the mechanism of destruction of the cylindrical sample in the Brazilian test*, [in:] *Advances in mechanics?: theoretical, computational and interdisciplinary issue*, [Eds: Kleiber M., Burczyński T., Wilde K., Górski J., Winkelmann K., Smakosz Ł.], pp. 479–483, Boca Raton, Gdańsk 2016,

12. Goodier J.N., *Compression of rectangular blocks, and the bending of beams by non-linear distributions of bending forces*, J. Appl. Mech., **54**(18): 173–183, 1932.

13. Mohammadi S., *Extended finite element method: for fracture analysis of structures*, Wiey-Blackwell, 2008.

14. Jirasek M., Zimmermann T., *Embedded crack model. Part II: Combination with smeared cracks*, International Journal for Numerical Methods in Engineering, **50**(6): 1291–1305, 2001, doi: 10.1002/1097-0207(20010228)50:6<1291::AID-NME12>3.0.CO;2-Q.

15. Tejchman J., Bobiński J., *Continuous and discontinuous modelling of fracture in concrete using FEM*, Springer-Verlag, 2013, doi: 10.1007/978-3-642-28463-2.

16. *Abaqus V 6.14.2 Users Manual*, 2014.

17. Bazant Z. P., Kazemi M. T., Hasegawa T., Mazars J., *Size effect in Brazilian split-cylinder tests. Measurements and fracture analysis*, ACI Materials Journal, **88**(3): 325–332, 1991.

18. Podgórski J., *The criterion for determining the direction of crack propagation in a random pattern composites*, Meccanica, **52**(8): 1923–1934, 2017, doi: 10.1007/s11012-016-0523-y.

Received December 23, 2018; accepted version July 7, 2019.
